Journal of Engineering Science 11(1), 2020, 01-08

JES
an international Journal

SYNTHESIS AND STRUCTURAL EVALUATION OF Mg, Cu, Zn TRI-DOPED LITHIUM TITANIUM OXIDE ELECTRODE MATERIALS FOR USE IN LITHIUM ION BATTERY

Parbhej Ahamed and Mohammad Abu Yousuf*

Department of Chemistry, Khulna University of Engineering & Technology, Khulna-9203, Bangladesh

Received: 25 January 2020 Accepted: 07 March 2020

ABSTRACT

Mg, Cu and Zn metals have been used to tri-dope into the tetrahedral and octahedral sites of $Li_4Ti_5O_{12}$ (LTO) electrode materials usually used in Li-ion battery. $Li_{4-x}Mg_xTi_{5-y}Zn_{y/2}Cu_{y/2}O_{12}$ (i. x = 0, y = 0 ii. x = 0.05, y=0.10 iii. x= 0.10, y= 0.20 iv. x= 0.15, y= 0.20) materials were synthesized by solid state reaction using the stoichiometric amount of raw materials. The structural and morphological characteristics of the tri-doped $Li_{4-x}Mg_xTi_{5-y}Zn_{y/2}Cu_{y/2}O_{12}$ materials were methodically analyzed by using Fourier transform infrared spectroscopy (FT-IR), UV-visible spectroscopy, thermogravimetric analysis (TGA), X-ray diffraction (XRD), scanning electron microscopic (SEM) techniques. The results of infrared spectroscopy exhibit bands of TO_6 octahedra and Ti-O-Ti vibrations. Band gap energy calculation from UV-visible spectroscopy demonstrates a critical point of doping. Beyond this point band gap energy has been found to increase upon tri-doping. It has been observed from SEM images that all samples possess micro-porous and coral shape structures. The XRD patterns demonstrate that Mg, Cu and Zn metals tri-doped $Li_{4-x}Mg_xTi_{5-y}Zn_{y/2}Cu_{y/2}O_{12}$ materials have spinel structure as well as good crystallinity.

Keywords: *$Li_4Ti_5O_{12}$; Doping; Lithium ion battery*

1. INTRODUCTION

Rechargeable lithium-ion batteries (LIBs) are extensively used as electrical energy storage systems and constitute critical elements in the development of sustainable energy technologies. The LIBs are currently being used in airplanes, electric vehicles, small appliances like laptops, mobile phones and in many other places (Scrosati *et al.,* 2010; Tarascon *et al.,* 2009; Yang *et al.,* 2009). They have proved to be a prominent energy storage technology in term of their high energy density, long cycle life, lighter weight and safety (Croguennec *et al.,* 2015). Over the years, the state of the art of the batteries based on the existing anode and cathode materials demand to find advance materials for high performance LIBs. Several electrode materials have been developed since the traditional carbon/graphite anode and $LiCoO_2$ cathode for LIBs (Dell *et al.,* 2000 and Endo *et al.,* 1996) which have been commercialized by Sony group in 1991.It is worthwhile to mention the names ofthe anode materials, such as graphite (Fong *et al.,* 1990), Si (Gómez *et al.,* 2015), Sn (Lübke *et al.,* 2015), $Li_4Ti_5O_{12}$ (Yi *et al.,* 2015), metal oxides like SnO_2(Li *et al.*, 2015), Co_3O_4(Wang *et al.,* 2015), NiO(Spinner*et al.,* 2015) used for this purposes.Among them spinel LTO has been found as one of the most promising anode materials for LIBsbecause ofits uniqueproperties. Many factors such as structural stability, longer life cycle, low cost and safety have been considered quite pertinent for use in LIB. It possesses good reversibility with almost negligible volume change during Li-ion insertion/extraction process and provides a good operating voltage at 1.5 V versus lithium. Despite assuming the aforementioned advantages, it exhibits poor electrical conductivity ($<10^{-13}$ S/cm) (Chen *et al.*, 2001; Guerfi *et al.,* 2004) as compared to the carbon (285 S/cm) (Li *et al.,* 2007). To solve the electrical conductivity limitation of LTO researchers have proposed various ways, such as synthesis of nano-sized LTO (Shen *et al.,* 2003), coating with conductive materials (Yuan *et al*., 2010) and doping with transition metals (Huang *et al.,* 2004) to shorten the diffusion distance of Li-ion in electrode. Among these methods, the doping offered a direct pathway for changing the material properties of LTO. It has been found that LTO was doped with metal ion such as Mg (Chen *et al.,* 2001), Zn (Yi *et al.,* 2012), Cu (Wang *et al.,* 2013), Al (Zhao *et al.,* 2008), Ta (Hu *et al.,* 2011), V (Yi *et al.,* 2009), Ag (Huang *et al.*, 2004), La (Gao *et al.,* 2010) etc. Moreover, there have been very few investigations dealing with tri-dopingof LTO structure with metal ions (Shenouda *et al.,* 2008). Accordingly, we have prepared Mg, Zn and Cu metals tri-doped $Li_{4-x}Mg_xTi_{5-y}Zn_{y/2}Cu_{y/2}O_{12}$ materials by solid state reactions. Structure evaluations of the as prepared $Li_{4-x}Mg_xTi_{5-y}Zn_{y/2}Cu_{y/2}O_{12}$ materials will now be presented here.

2. EXPERIMENTAL

2.1 Sample Preparation

Solid state reaction method was used to prepare $Li_{4-x}Mg_xTi_{5-y}Zn_{y/2}Cu_{y/2}O_{12}$ (i. x = 0, y = 0 ii. x= 0.05, y=0.10 iii.

* Corresponding Author: yousuf@chem.kuet.ac.bd
ISSN 2075-4914 (print); ISSN 2706-6835 (online)

x= 0.10, y= 0.20 iv. X= 0.15, y= 0.20) compounds. $LiOH.H_2O$ (Merck, Germany), TiO_2 (Merck, Germany), $Mg(NO_3)_2.6H_2O$ (Merck, Germany), $Cu(NO_3)_2.3H_2O$ (Merck, Germany) and $Zn(NO_3)_2.6H_2O$ (Loba Chemie, India) were used without further purification as starting raw materials to prepare $Li_{4-x}Mg_xTi_{5-y}Zn_{y/2}Cu_{y/2}O_{12}$ materials. Stoichiometric quantities of the starting materials were well grounded using agate pestle and mortar for about half an hour to obtaina homogeneous mixture of the raw materials. Then, the mixture was transferred into a crucible and heated in a muffle furnace at 750ºC for 6 hours. After calcinations the product $Li_{4-x}Mg_xTi_{5-y}Zn_{y/2}Cu_{y/2}O_{12}$was grounded using agate mortar and kept in desiccators for characterization.

2.2 Fourier Transform Infrared Spectroscopy (FT-IR)

$Li_{4-x}Mg_xTi_{5-y}Zn_{y/2}Cu_{y/2}O_{12}$ materials were well finely grinded with KBr and pressed into pellets using a manual hydraulic pressfor FT-IR measurements. IR Tracer-100 of Shimadzu Corporation, Japan, was used to record the FT-IR spectra. The pellet was scanned in the wave number range of 500-4000 cm^{-1} with a 2 cm^{-1} resolution.

2.3 UV-visible Spectroscopy

Appropriate amount of $Li_{4-x}Mg_xTi_{5-y}Zn_{y/2}Cu_{y/2}O_{12}$ samples were suspended inethanol in a cuvette. The cuvette was then placed into its holder for recording UV-visible spectra of the respective sample. UV-1800 spectrophotometer of Shimadzu Corporation, Japan, was used to measure the sample absorption spectra in the range 200-800 nm. Band gap for each of each sample was their respective absorption spectra using Tauc plot.

2.4 Scanning Electron Microscopy (SEM)

Morphology of the prepared $Li_{4-x}Mg_xTi_{5-y}Zn_{y/2}Cu_{y/2}O_{12}$ materials was determined using scanning electron microscopy technique. Prepared samples were suspended in ethanol. Alumina plate was used to adhere conductive carbon tape. 2-3 drops of the suspended sample were added on the surface of the conductive carbon tape. It was then allowed to dry for a sufficient period of time. After drying air blower was used to remove excess powder from the sample plate. The sample plate was finally placed on the chamber for SEM operation.

2.5 Powder X-ray diffraction (XRD)

Bruker Advance D8 XRD diffractometer equipped with a CuK_α monochromatic beam (λ = 0.15406Å) was used to identify the phases present in the prepared $Li_{4-x}Mg_xTi_{5-y}Zn_{y/2}Cu_{y/2}O_{12}$ materials. Sample holders of the diffractometer was loaded by pouring with $Li_{4-x}Mg_xTi_{5-y}Zn_{y/2}Cu_{y/2}O_{12}$ materials. It was then mounted on the diffractometer and scanned from 0 to 80º.

2.6 Calculation of x-ray density, bulk density, grain size and porosity

More structural information of the synthesized $Li_{4-x}Mg_xTi_{5-y}Zn_{y/2}Cu_{y/2}O_{12}$ materials was calculated using the following equation.

X-ray density, $$\rho_x = \frac{ZM}{Na^3} \quad (1)$$

where M is the molecular weight of the corresponding composition, N is the Avogadro's number (6.023×10^{23}), "a" is the lattice parameter and Z is the number of molecules per unit cell.

Bulk density, $$\rho_b = \frac{m}{V} \quad (2)$$

where m is the mass of the sample, V is the volume of the sample.

Grain size, $$D_g = \frac{0.9\,\lambda}{\beta \cos\theta} \quad (3)$$

where, D_g is the crystal size; λ is the wavelength of the X-ray radiation (λ=0.15406 nm) for Cu K_α and β is the linewidth at half-maximum height.

$$\text{Porosity} = \left(1 - \frac{\rho_b}{\rho_x}\right) \times 100\ \% \quad (4)$$

The difference between the bulk density, ρ_b and X-ray density, $\rho_x$was considered as a measure of the porosity of the material synthesized.

3. RESULTS AND DISCUSSION

FT-IR spectra of $Li_{4-x}Mg_xTi_{5-y}Zn_{y/2}Cu_{y/2}O_{12}$ materials are shown in Figure 1. The presence of a broad peak in the spectra can be observed at 3428 cm^{-1}. This resulted from the -OH stretching vibrations of the free and hydrogen bonded surface hydroxyl group.The bands near 1650 cm^{-1} is assigned to the bending stretching vibration of –OH groups (Liu *et al*., 2006). The absorption bands due to –OH are related to the absorption of water molecules during the preparation of the KBr pellet. Peaks close to 1400 cm^{-1} are due to the vibrations of CO_3^{2-} anion (Zhang *et al.,* 2007). Appearance of peaks at 2850 to 2900 cm^{-1} is due to the presence of C–H stretching of –

CH_2– or $–CH_3$ group. Peaks located near 2330 and 1050 cm^{-1} are due to the vibration of Ti-O bond and TiO_6 octahedra (Zhang *et al.,* 2007 and Li *et al.,* 2008), respectively. UV-visible absorption spectra of the prepared $Li_{4-x}Mg_xTi_{5-y}Zn_{y/2}Cu_{y/2}O_{12}$ materials are presented in Figure 2.

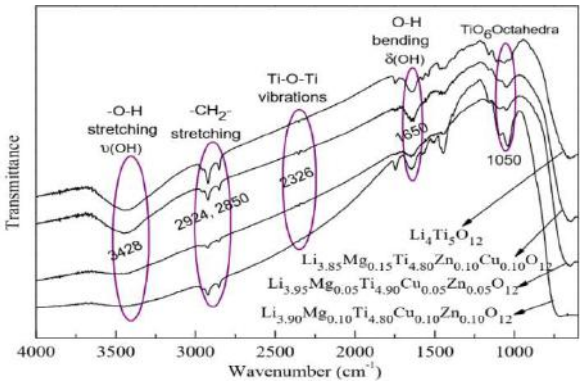

Figure 1: FTIR spectrum of the prepared $Li_{4-x}Mg_xTi_{5-y}Zn_{y/2}Cu_{y/2}O_{12}$ materials

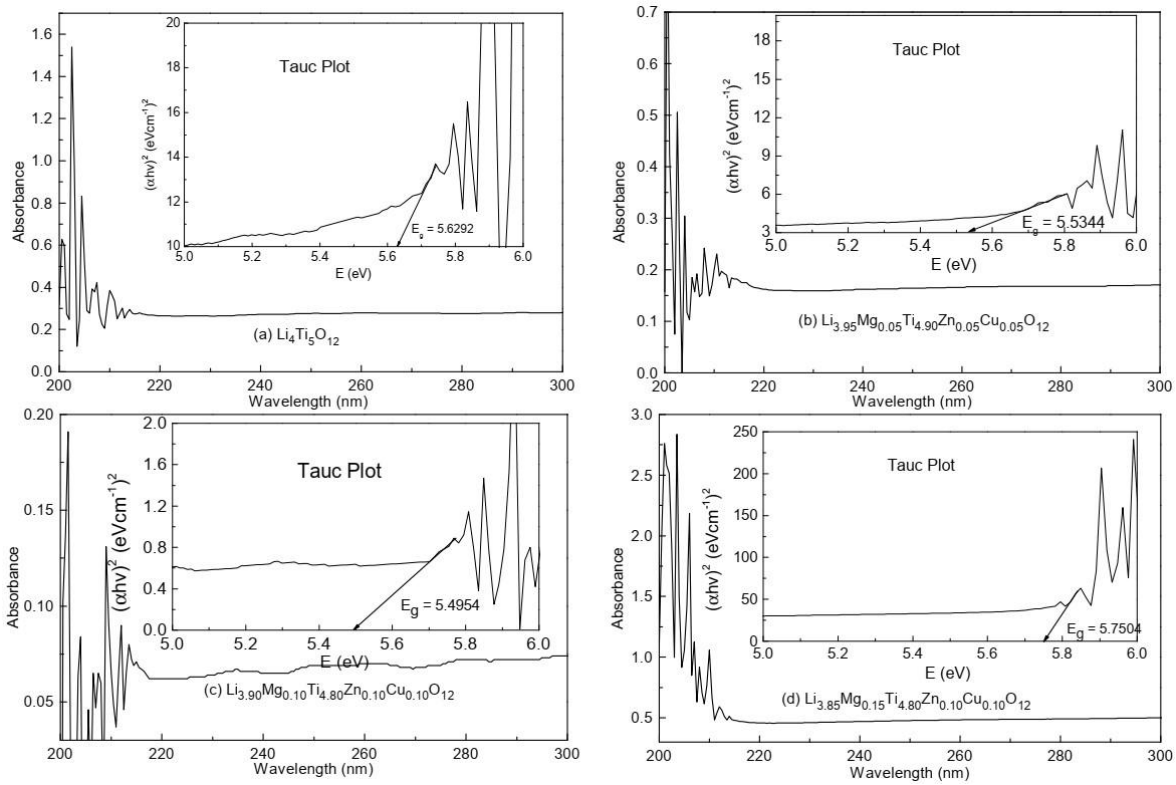

Figure 2: UV-visible spectra of the prepared $Li_{4-x}Mg_xTi_{5-y}Zn_{y/2}Cu_{y/2}O_{12}$ materials (a) $Li_4Ti_5O_{12}$, (b) $Li_{3.95}Mg_{0.05}Ti_{4.90}Cu_{0.05}Zn_{0.05}O_{12}$, (c) $Li_{3.90}Mg_{0.10}Ti_{4.80}Cu_{0.10}Zn_{0.10}O_{12}$ and (d) $Li_{3.85}Mg_{0.15}Ti_{4.80}Zn_{0.10}Cu_{0.10}O_{12}$

Table 1: Band gap energy $Li_{4-x}Mg_xTi_{5-y}Zn_{y/2}Cu_{y/2}O_{12}$ anode materials

Sample	Band gap energy, E (eV)
$Li_4Ti_5O_{12}$(LTO)	5.6292
$Li_{3.95}Mg_{0.05}Ti_{4.90}Cu_{0.05}Zn_{0.05}O_{12}$(LTOM1)	5.5344
$Li_{3.90}Mg_{0.10}Ti_{4.80}Cu_{0.10}Zn_{0.10}O_{12}$ (LTOM2)	5.4954
$Li_{3.85}Mg_{0.15}Ti_{4.80}Zn_{0.10}Cu_{0.10}O_{12}$ (LTOM3)	5.7504

Band gap energy of $Li_{4-x}Mg_xTi_{5-y}Zn_{y/2}Cu_{y/2}O_{12}$ materials was calculated by extrapolation of the Tauc plot. The calculated band gap energies are summarized in the following Table 1. Tri-doping of $Li_{4-x}Mg_xTi_{5-y}Zn_{y/2}Cu_{y/2}O_{12}$ materials has decreased the band gap energies except $Li_{3.85}Mg_{0.15}Ti_{4.80}$ $Zn_{0.10}Cu_{0.10}O_{12}$. It is obvious that

lowering of band gaps of tri-doped $Li_{4-x}Mg_xTi_{5-y}Zn_{y/2}Cu_{y/2}O_{12}$ materials have resulted from the larger radius of the dopant ions (Mg^{2+} = 86 pm, Zn^{2+} = 88 pm, Cu^{2+} = 87 pm) compared to the host ions (Li^{+} = 90 pm, Ti^{4+} = 74.5 pm). In the $Li_4Ti_5O_{12}$ compound, the valence band (VB) and the conduction band (CB) consist of Li 2s, Ti 3d and O 2p orbitals. When $Li_4Ti_5O_{12}$ compound is tri-doped with Mg, Cu, Zn metals, and the valence state of tri-doped $Li_{4-x}Mg_xTi_{5-y}Zn_{y/2}Cu_{y/2}O_{12}$ compound subsequently become more delocalized with Mg 2p, Cu 3d and Zn 3d orbital'sresulting mixing of Mg 2p, Cu 3d and Zn 3d state with VB, and thus increases the width of the VB itself. A plot of band gap energy with doping in tri-doped $Li_{4-x}Mg_xTi_{5-y}Zn_{y/2}Cu_{y/2}O_{12}$ is presented in Figure 3. It is obvious that the band gap energy of the tri-doped $Li_{4-x}Mg_xTi_{5-y}Zn_{y/2}Cu_{y/2}O_{12}$ materials has decreased up to a certain amount of dopants.

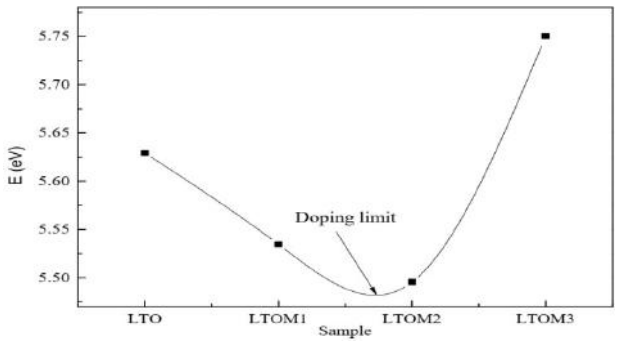

Figure 3: Variation of band gap energy in $Li_{4-x}Mg_xTi_{5-y}Zn_{y/2}Cu_{y/2}O_{12}$

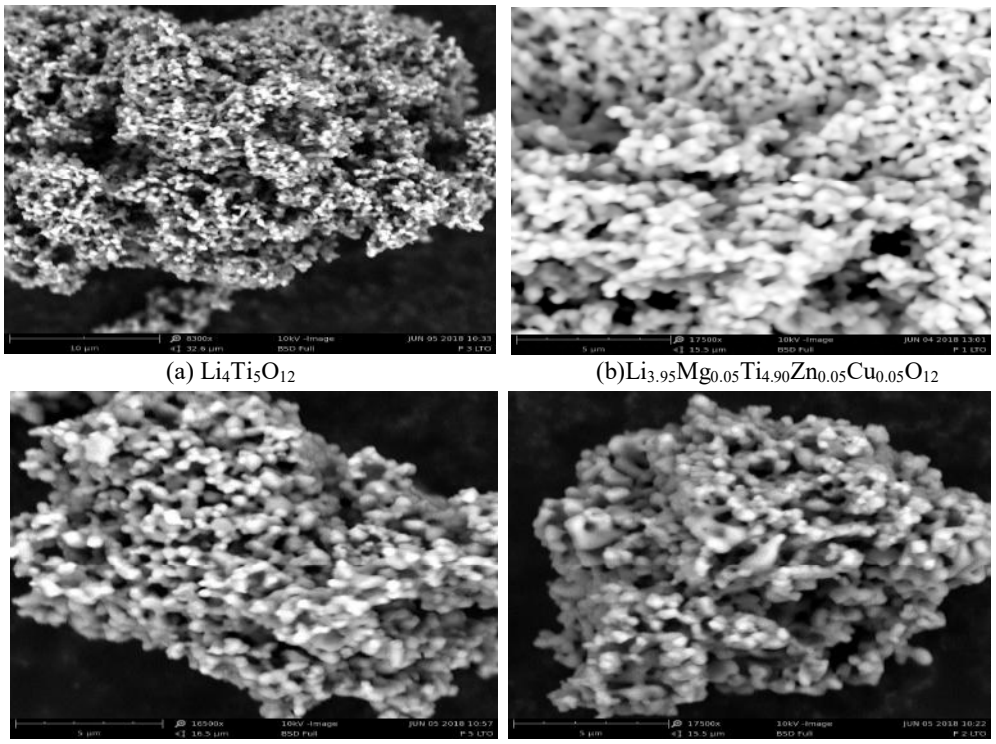

(a) $Li_4Ti_5O_{12}$ (b)$Li_{3.95}Mg_{0.05}Ti_{4.90}Zn_{0.05}Cu_{0.05}O_{12}$

(c) $Li_{3.90}Mg_{0.10}Ti_{4.80}Zn_{0.10}Cu_{0.10}O_{12}$ (d) $Li_{3.85}Mg_{0.15}Ti_{4.80}Zn_{0.10}Cu_{0.10}O_{12}$

Figure 4: SEM images of the prepared sample $Li_{4-x}Mg_xTi_{5-y}Zn_{y/2}Cu_{y/2}O_{12}$.

Then it increased with increasing the amount of doping. This behavior is expected because of the incorporation of dopant into the crystal lattice. With increasing the amount of dopant some of them could not completely incorporate into the spinel structure of $Li_4Ti_5O_{12}$. As a result, the interaction between the cations and anions might have been changed. This ultimately affects the electronic state of the valence band of $Li_{4-x}Mg_xTi_{5-y}Zn_{y/2}Cu_{y/2}O_{12}$ materials. Eventually it generates the anomalies in the band gap of Mg, Cu, and Zn tri-doped of $Li_{4-x}Mg_xTi_{5-y}Zn_{y/2}Cu_{y/2}O_{12}$ compounds.

The surface morphology of the prepared $Li_{4-x}Mg_xTi_{5-y}Zn_{y/2}Cu_{y/2}O_{12}$ materials was investigated by scanning electron microscopy (SEM). Figure 4 shows the representative SEM images of the prepared materials. It is

interesting to note that the morphology of the tri-doped samples has hardly changed. Morphology of the tri-doped sample is very similar to the un-doped samples. Based on this observation it is concluded that metals are homogeneously tri-doped into $Li_{4-x}Mg_xTi_{5-y}Zn_{y/2}Cu_{y/2}O_{12}$. All the prepared samples exhibit micro-porous and coral shape structures. This coral shape structure is associated with sufficient pores. Each of these pores may offer short pathways for Li-ion diffusion. Furthermore, the well decorated pores of the coral structures may act as active sites and provide more ion channels for extraction or insertion processes of Li-ion into $Li_{4-x}Mg_xTi_{5-y}Zn_{y/2}Cu_{y/2}O_{12}$ materials. Thus, each of these $Li_{4-x}Mg_xTi_{5-y}Zn_{y/2}Cu_{y/2}O_{12}$ materials having sufficient active sites and diffusion channels may be used as electrode materials in Li-ion battery.

Figure 5 shows the representative XRD patterns of the prepared $Li_{4-x}Mg_xTi_{5-y}Zn_{y/2}Cu_{y/2}O_{12}$ samples. All the diffraction peaks can be well indexed to a cubic spinel structure of $Li_4Ti_5O_{12}$ (JCPDS card No. 00-049-0207). No peaks from impurities are observed. This indicates that the metals have been successfully entered into the lattice of $Li_{4-x}Mg_xTi_{5-y}Zn_{y/2}Cu_{y}2O_{12}$.

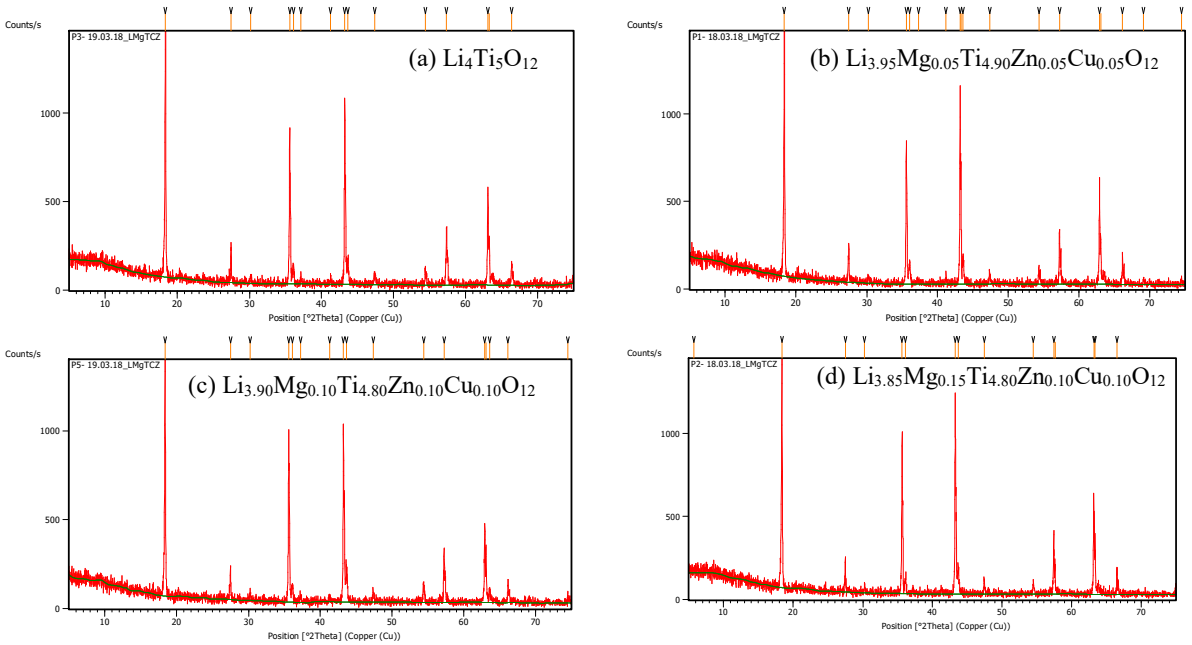

Figure 5: XRD spectra of the prepared samples $Li_{4-x}Mg_xTi_{5-y}Zn_{y/2}Cu_{y/2}O_{12}$

Diffraction peaks of the prepared $Li_{4-x}Mg_xTi_{5-y}Zn_{y/2}Cu_{y/2}O_{12}$ samples can be indexed as (111), (220), (311), (400), (331), (333), (440) and (531) of the cubic $Li_4Ti_5O_{12}$ (Guo *et al*., 2015). This confirmed that tri-doping do not change the basic structure of $Li_4Ti_5O_{12}$. Then the aforementioned indexed planes were used to calculate interplanar spacing, lattice constant and grain sizes of the prepared $Li_{4-x}Mg_xTi_{5-y}Zn_{y/2}Cu_{y/2}O_{12}$ samples. The calculated structural parameters from the analysis of the XRD patterns are summarized in the following Table 2.

The lattice parameters of $Li_{4-x}Mg_xTi_{5-y}Zn_{y/2}Cu_{y/2}O_{12}$ materials are calculated through the Bragg's equation from the diffraction peaks of (111), (220), (311), (400), (331), (333), (440) and (531) planes. The average lattice parameters obtained by analysis of the X-ray pattern werefound to be 8.3545Å for $Li_4Ti_5O_{12}$, 8.3597 Å for $Li_{3.95}Mg_{0.05}Ti_{4.90}Zn_{0.05}Cu_{0.05}O_{12}$, 8.3585Å for $Li_{3.90}Mg_{0.10}Ti_{4.80}Zn_{0.10}Cu_{0.10}O_{12}$, 8.3427 Å for $Li_{3.85}Mg_{0.15}Ti_{4.80}Zn_{0.10}Cu_{0.10}O_{12}$. Moreover, the variation in the calculated lattice parameter and unit cell volume of the tri-doped $Li_{4-x}Mg_xTi_{5-y}Zn_{y/2}Cu_{y/2}O_{12}$ materials are presented in Figure 6.

Lattice parameters for $Li_{3.95}Mg_{0.05}Ti_{4.90}Zn_{0.05}Cu_{0.05}O_{12}$ and $Li_{3.90}Mg_{0.10}Ti_{4.80}Zn_{0.10}Cu_{0.10}O_{12}$ composition has been found to increase than that of $Li_4Ti_5O_{12}$. This increase of lattice parameter resulted from the larger radius of the dopant ions (Mg^{2+} = 86 pm, Zn^{2+} = 88 pm, Cu^{2+} = 87 pm) compared to the host ions (Li^{+} = 90 pm, Ti^{4+} = 74.5 pm) (Lu *et al*., 2016). The unit cell volume of the tri-doped $Li_{4-x}Mg_xTi_{5-y}Zn_{y/2}Cu_{y/2}O_{12}$ materials has been distorted upon changing the dopant amount. Mismatch of the unit cell volume due to doping can be represented as shown in the following Figure 6.

More structural information related to the crystal structure of $Li_{4-x}Mg_xTi_{5-y}Zn_{y/2}Cu_{y/2}O_{12}$ materials has been calculated using equation (1), (2) (3) and (4). The values of X-ray density, bulk density and percentage of porosity obtained using equation (1), (2) and (4), respectively are listed in Table 3. X-ray density $\rho_x$of the tri-doped $Li_{4-x}Mg_xTi_{5-y}Zn_{y/2}Cu_{y/2}O_{12}$ increased with increasing dopant concentrations. The substitution of low

atomic mass Li and Ti with large atomic mass Mg, Cu and Zn in accordance with the enhancement of X-ray density of tri-doped $Li_{4-x}Mg_xTi_{5-y}Zn_{y/2}Cu_{y/2}O_{12}$. In contrast, the calculated values of bulk density of tri-doped $Li_{4-x}Mg_xTi_{5-y}Zn_{y/2}Cu_{y/2}O_{12}$ decreased with increasing the concentration of dopants. Results of the X-ray density and bulk density have been used to calculate the percentage of porosity present in the tri-doped $Li_{4-x}Mg_xTi_{5-y}Zn_{y/2}Cu_{y/2}O_{12}$. It can be seen from Table 3 that the percentage of porosity increased with increasing the dopant concentration. The variation of density with Mg, Cu and Zn content in $Li_{4-x}Mg_xTi_{5-y}Zn_{y/2}Cu_{y/2}O_{12}$ are depicted in Figure 7(a). Variation in the percentage of porosity present in $Li_{4-x}Mg_xTi_{5-y}Zn_{y/2}Cu_{y/2}O_{12}$ materials is also presented in the Figure 7(b).

Table 2: Position of the X-ray peaks, interplanar spacing, corresponding miller indices and grainsize of each plane

$Li_4Ti_5O_{12}$	2θ	18.345	30.183	35.578	43.266	47.417	57.348	63.097	66.376
	d (Å)	4.8361	2.9609	2.5234	2.0911	1.9173	1.6053	1.4722	1.4072
	(hkl)	(111)	(220)	(311)	(400)	(331)	(333)	(440)	(531)
	a	8.3763	8.3746	8.3691	8.3644	8.3573	8.3413	8.3280	8.3251
	a_{avg}(Å)				8.3545				
	V (Å)^3				583.12				
	D_g (nm)	68	34	105	108	55	188	97	65
	$D_{g,\,avg}$ (nm)				90				
$Li_{3.95}Mg_{0.05}Ti_{4.90}Zn_{0.05}Cu_{0.05}O_{12}$	2θ	18.357	30.241	35.573	43.237	47.381	57.247	62.886	66.142
	d (Å)	4.8330	2.9554	2.5237	2.0907	1.9171	1.6079	1.4766	1.4116
	(hkl))	(111)	(220)	(311)	(400)	(331)	(333)	(440)	(531)
	a	8.3710	8.3591	8.3701	8.3628	8.3564	8.3548	8.3529	8.3511
	a_{avg}(Å)				8.3597				
	V (Å)^3				584.21				
	D_g (nm)	81	41	60	88	60	94	97	131
	$D_{g,\,avg}$ (nm)				82				
$Li_{3.90}Mg_{0.10}Ti_{4.80}Zn_{0.10}Cu_{0.10}O_{12}$	2θ	18.392	30.237	35.593	43.264	47.389	57.263	62.909	66.150
	d (Å)	4.8238	2.9558	2.5223	2.0912	1.9183	1.6088	1.4764	1.4114
	(hkl)	(111)	(220)	(311)	(400)	(331)	(333)	(440)	(531)
	a	8.3550	8.3602	8.3655	8.3648	8.3616	8.3595	8.3517	8.3499
	a_{avg}(Å)				8.3585				
	V (Å)^3				583.96				
	D_g (nm)	68	69	84	108	36	91	97	78
	$D_{g,\,avg}$ (nm)				79				
$Li_{3.85}Mg_{0.15}Ti_{4.80}Zn_{0.10}Cu_{0.10}O_{12}$	2θ	18.389	30.245	35.617	43.314	47.457	57.428	63.185	66.488
	d (Å)	4.8246	2.9550	2.5207	2.0889	1.9158	1.6033	1.4703	1.4051
	(hkl)	(111)	(220)	(311)	(400)	(331)	(333)	(440)	(531)
	a (Å)	8.3564	8.3580	8.3602	8.3556	8.3507	8.3309	8.3172	8.3126
	a_{avg}(Å)				8.3427				
	V (Å)^3				580.65				
	D_g (nm)	81	69	105	86	73	75	97	131
	$D_{g,\,avg}$ (nm)				90				

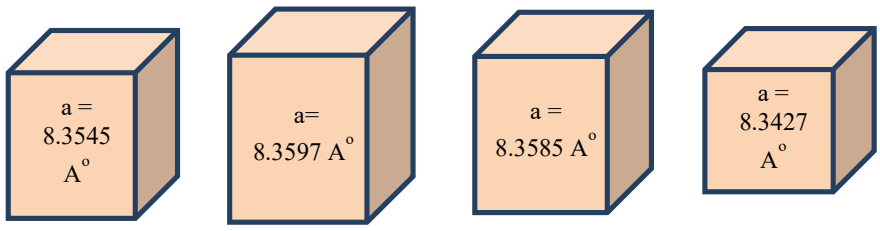

(a) LTO (b) LTOM1 (c) LTOM2 (d) LTOM3

Figure 6: Mismatch of cubic unit cell of $Li_{4-x}Mg_xTi_{5-y}Zn_{y/2}Cu_{y/2}O_{12}$due to doping

Table 3: X-ray density, bulk density and porosity of the prepared samples

Sample	X-ray density, ρ_x (g/cm^3)	Bulk density, ρ_b (g/cm^3)	Porosity (%)
$Li_4Ti_5O_{12}$	10.080	1.010	89.98
$Li_{3.95}Mg_{0.05}Ti_{4.90}Zn_{0.05}Cu_{0.05}O_{12}$	10.112	0.976	90.64
$Li_{3.90}Mg_{0.10}Ti_{4.80}Zn_{0.10}Cu_{0.10}O_{12}$	10.576	0.954	90.97
$Li_{3.85}Mg_{0.15}Ti_{4.80}Zn_{0.10}Cu_{0.10}O_{12}$	10.617	0.944	91.10

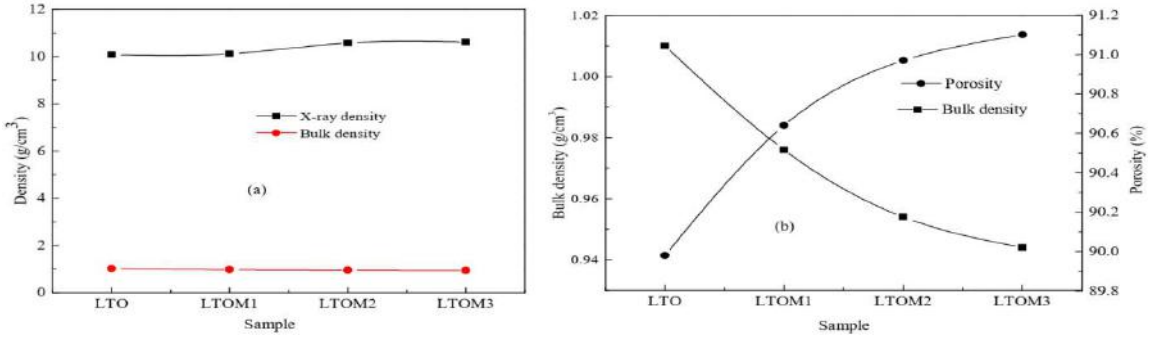

Figure 7: Variation of (a) bulk density and X-ray density and (b) bulk density and porosity of the tri-dope $Li_{4-x}Mg_xTi_{5-y}Zn_{y/2}Cu_{y/2}O_{12}$ materials

4. CONCLUSION

Micro-porous and coral shape $Li_{4-x}Mg_xTi_{5-y}Zn_{y/2}Cu_{y/2}O_{12}$ (i. x = 0, y = 0 ii. x= 0.05, y=0.10 iii. x= 0.10, y= 0.20 iv. X= 0.15, y= 0.20) compounds were prepared by solid state reaction method. XRD analysis revealed that Mg, Cu and Zn were tri-doped into $Li_{4-x}Mg_xTi_{5-y}Zn_{y/2}Cu_{y/2}O_{12}$ structure. The tri-doping of Mg, Cu and Zn metals into $Li_{4-x}Mg_xTi_{5-y}Zn_{y/2}Cu_{y/2}O_{12}$ structure depends upon a certain value of x and y and beyond that value inhibit complete incorporation into $Li_4Ti_5O_{12}$ structure. Minimum band gap energy of Mg, Cu and Zn tri-doped $Li_{4-x}Mg_xTi_{5-y}Zn_{y/2}Cu_{y/2}O_{12}$ resulted from the saturated amount of dopants. Band gap energy of Mg, Cu and Zn tri-doped $Li_{4-x}Mg_xTi_{5-y}Zn_{y/2}Cu_{y/2}O_{12}$ are found to decrease to certain amount of the dopant. Then it increased with increasing the amount of dopant. $Li_4Ti_5O_{12}$ as well as Mg, Cu and Zn tri-doped $Li_{4-x}Mg_xTi_{5-y}Zn_{y/2}Cu_{y/2}O_{12}$ shows micro-porous and coral shape morphology. Diffraction peaks from XRD spectra represented cubic spinel structure of $Li_{4-x}Mg_xTi_{5-y}Zn_{y/2}Cu_{y/2}O_{12}$ materials. A linear variation of X-ray density, bulk density and percentage of porosity with increasing the amount of dopant has been observed in the tri-doped $Li_{4-x}Mg_xTi_{5-y}Zn_{y/2}Cu_{y/2}O_{12}$ materials.

ACKNOWLEDGEMENT

The authors are thankful to the Committee for Advanced Studies and Research of Khulna University of Engineering & Technology for providing fund of this research.

CONFLICT OF INTERESTS

The authors declare that they have no conflict of interests.

REFERENCES

Chen, C. H., Vaughey J. T., Jansen A. N., Dees D. W., Kahaian A. J., Goacher T., and Thackeray M. M., 2001. Studies of Mg-Substituted $Li_{4-x}Mg_xTi_5O_{12}$ Spinel Electrodes (0 ≤x≤1) for Lithium Batteries, *Journal of the Electrochemical Society*, ***148***(1), A102-A104

Croguennec, L., and Palacin M. R., 2015. Recent achievements on inorganic electrode materials for lithium-ion batteries, *Journal of the American Chemical Society*, ***137***(9), 3140-3156

Dell, R. M., 2000. Batteries: fifty years of materials development, *Solid State Ionics*, ***134***(1-2), 139-158

Dupont, L., 2009. Hunting for better Li-based electrode materials via low temperature inorganic synthesis, *Chemistry of Materials*, ***22***(3), 724-739

Endo, M., Nishimura Y., Takahashi T., Takeuchi K., and Dresselhaus M. S., 1996. Lithium storage behavior for various kinds of carbon anodes in Li ion secondary battery, *Journal of Physics and Chemistry of Solids*, ***57***(6-8), 725-728

Fong, R., Von Sacken U., and Dahn J. R., 1990. Studies of lithium intercalation into carbons using nonaqueous electrochemical cells, *Journal of The Electrochemical Society*, ***137***(7), 2009-2013

Ferg, E., Gummow R. J., De Kock A., and Thackeray M. M., 1994. Spinel anodes for lithium□ion batteries *Journal of the Electrochemical Society*, ***141***(11), L147-L150

Guerfi, A., Charest P., Kinoshita K., Perrier M., and Zaghib K., 2004. Nano electronically conductive titanium-spinel as lithium ion storage negative electrode, *Journal of Power Sources*, ***126***(1-2), 163-168

Gao, J., Jiang C., and Wan C., 2010. Synthesis and characterization of spherical La-doped nanocrystalline $Li_4Ti_5O_{12}$/C compound for lithium-ion batteries, *Journal of The Electrochemical Society*, ***157***(2), K39-K42

Gómez-Cámer, J.L., Thuv H., and Novák P., 2015. Electrochemical study of Si/C composites with particulate and fibrous morphology as negative electrodes for lithium-ion batteries, *Journal of Power Sources*, *294*, 128-135

Guo, M., Wang S., Ding L.X., Huang C., and Wang H., 2015. Tantalum-doped lithium titanate with enhanced performance for lithium-ion batteries, *Journal of Power Sources,* 283, 372-380

Huang, S., Wen Z., Zhu X., and Gu Z., 2004. Preparation and electrochemical performance of Ag doped $Li_4Ti_5O_{12}$, *Electrochemistry Communications*, ***6***(11), 1093-1097

Hu, G. R., Zhang X. L., and Peng Z. D., 2011. Preparation and electrochemical performance of tantalum-doped lithium titanate as anode material for lithium-ion battery, *Transactions of Nonferrous Metals Society of China*, ***21***(10), 2248-2253

Li, Q. W., Li Y., Zhang X. F., Chikkannanavar S.B., Zhao Y.H., Dangelewicz A.M., Zheng L.X., Doorn S.K., Jia Q.X., Peterson D.E., and Arendt P.N., 2007. Structure□dependent electrical properties of carbon nanotube fibers, *Advanced Materials*, ***19***(20), 3358-3363

Li, Y., Zhao H., Tian Z., Qiu W., and Li X., 2008. Solvothermal synthesis and electrochemical characterization of amorphous lithium titanate materials, *Journal of alloys and compounds,* 455(1-2), 471-474

Li, W., Yoon D., Hwang J., Chang W., and Kim J., 2015. One-pot route to synthesize SnO_2-reduced graphene oxide composites and their enhanced electrochemical performance as anodes in lithium-ion batteries, *Journal of Power Sources*, *293*, 1024-1031

Liu, X., Jia P., Lin J., and Li G., 2006. Monodisperse spherical core-shell structured SiO_2–$CaTiO_3$: Pr^{3+} phosphors for field emission displays, Journal of applied physics, **99**(12), 124902

Lu, P., Huang X., Ren Y., Ding J., Wang H., Zhou S., Chen Y., and Ding X., 2016. Na^+ and Zr^{4+} co-doped $Li_4Ti_5O_{12}$ as anode materials with superior electrochemical performance for lithium ion batteries, Rsc Advances, **6**(93), 90455-90461

Lübke, M., Johnson I., Makwana N. M., Brett D., Shearing P., Liu Z., and Darr J. A., 2015. High power TiO_2 and high capacity Sn-doped TiO_2 nanomaterial anodes for lithium-ion batteries, *Journal of Power Sources*, *294*, 94-102.

Qi, Y., Huang Y., Jia D., Bao S.J., and Guo Z.P., 2009. Preparation and characterization of novel spinel $Li_4Ti_5O_{12-x}Br_x$ anode materials, *Electrochimica Acta*, ***54***(21), 4772-4776

Shen, C. M., Zhang X. G., Zhou Y. K., and Li H. L., 2003. Preparation and characterization of nanocrystalline $Li_4Ti_5O_{12}$ by sol–gel method, *Materials chemistry and physics*, ***78***(2), 437-441

Shenouda, A. Y., and Murali K. R., 2008. Electrochemical properties of doped lithium titanate compounds and their performance in lithium rechargeable batteries, *Journal of Power Sources*, ***176***(1), 332-339

Scrosati, B., and Garche J., 2010. Lithium batteries: Status, prospects and future, *Journal of power sources*, **195**(9), 2419-2430

Spinner, N.S., Palmieri A., Beauregard N., Zhang L., Campanella J., and Mustain W. E., 2015. Influence of conductivity on the capacity retention of NiO anodes in Li-ion batteries, *Journal of Power Sources*, *276*, 46-53

Tarascon, J. M., Recham N., Armand M., Chotard J. N., Barpanda P., Walker W., and Dupont L., 2009. Hunting for better Li-based electrode materials via low temperature inorganic synthesis, *Chemistry of Materials,* **22**(3), 724-739

Wang, J., Zhao H., Yang Q., Zhang T., and Wang J., 2013. Electrochemical characteristics of $Li_{4-x}Cu_xTi_5O_{12}$ used as anode material for lithium-ion batteries, *Ionics*, ***19***(3), 415-419

Wang, Y., Wang B., Xiao F., Huang Z., Wang Y., Richardson C., Chen Z., Jiao L., and Yuan H., 2015. Facile synthesis of nanocage Co_3O_4 for advanced lithium-ion batteries, *Journal of Power Sources*, *298*, 203-208

Yang, Z., Choi D., Kerisit S., Rosso K. M., Wang D., Zhang J., Graff G., and Liu J., 2009. Nanostructures and lithium electrochemical reactivity of lithium titanites and titanium oxides: A review, *Journal of Power Sources*, ***192***(2), 588-598

Yi, T.F., Shu J., Zhu Y. R., Zhu X. D., Yue C.B., Zhou A. N., and Zhu R. S., 2009. High-performance $Li_4Ti_{5-x}V_xO_{12}$ ($0 \leq x \leq 0.3$) as an anode material for secondary lithium-ion battery, *Electrochimica Acta*, ***54***(28), 7464-7470

Yuan, T., Yu X., Cai R., Zhou Y., and Shao Z., 2010. Synthesis of pristine and carbon-coated $Li_4Ti_5O_{12}$ and their low-temperature electrochemical performance, *Journal of Power Sources*, ***195***(15), 4997-5004

Yi, T.F., Liu H., Zhu Y. R., Jiang L. J., Xie Y., and Zhu R. S., 2012. Improving the high rate performance of $Li_4Ti_5O_{12}$ through divalent zinc substitution, *Journal of Power Sources*, *215*, 258-265

Yi, T. F., Yang S. Y., and Xie Y., 2015. Recent advances of $Li_4Ti_5O_{12}$ as a promising next generation anode material for high power lithium-ion batteries, *Journal of Materials Chemistry A*, ***3***(11), 5750-5777

Zhang, D. R., Liu H. L., Jin R. H., Zhang N. Z., Liu Y. X., and Kang Y. S., 2007. Synthesis and characterization of nanocrystalline $LiTiO_2$ using a one-step hydrothermal method, *Journal of Industrial and Engineering Chemistry,* **13**(1), 92-96

Zhao, H., Li Y., Zhu Z., Lin J., Tian Z., and Wang R., 2008. Structural and electrochemical characteristics of $Li_{4-x}Al_xTi_5O_{12}$ as anode material for lithium-ion batteries, *Electrochimica Acta*, ***53***(24), 7079-7083